LAWRENCE
LIVERMORE
NATIONAL
LABORATORY

LLNL-JRNL-402318

Hyperfine Quenching of the 2s2p 3P0 State of Berylliumlike Ions

K. T. Cheng, M. H. Chen, W. R. Johnson

March 17, 2008

Physical Review A

Disclaimer

Hyperfine quenching of the $2s2p\,^3P_0$ state of berylliumlike ions

K. T. Cheng (鄭國錚)* and M. H. Chen (陳茂雄)†

Lawrence Livermore National Laboratory, Livermore, CA 94550

W. R. Johnson‡

Department of Physics, University of Notre Dame, Notre Dame, IN 46556

(Dated: March 13, 2008)

Abstract

The hyperfine-induced $2s2p\,^3P_0 - 2s^2\,^1S_0$ transition rate for Be-like $^{47}Ti^{18+}$ was recently measured in a storage-ring experiment by Schippers *et al.* [Phys. Rev. Lett. **98**, 033001 (2007)]. The measured value of 0.56(3) s^{-1} is almost 60% larger than the theoretical value of 0.356 s^{-1} from a multiconfiguration Dirac-Fock calculation by Marques *et al.* [Phys. Rev. A **47**, 929 (1993)]. In this work, we use a large-scale relativistic configuration-interaction method to calculate these hyperfine-induced rates for ions with $Z = 6 - 92$. Coherent hyperfine-quenching effects between the $2s2p\,^{1,3}P_1$ states are included in a perturbative as well as a radiation damping approach. Contrary to the claims of Marques *et al.*, contributions from the $^1P_1$ state are substantial and lead to a hyperfine-induced rate of 0.67 s^{-1}, in better agreement with, though larger than, the measured value.

PACS numbers: 31.30.Jv, 32.30.Rj, 31.25.-v, 31.15.Ar

*ktcheng@llnl.gov

†chen7@llnl.gov

‡johnson@nd.edu

I. INTRODUCTION

The $2s2p\,^3P_0$ state is the lowest excited state in Be-like ions. This metastable state is forbidden to decay to the $2s^2\,^1S_0$ ground state by an one-photon transition because $J = 0 - 0$ transition is strictly forbidden by angular selection rules, and the two-photon E1-M1 transition is extremely weak. However, for isotopes with nonzero nuclear spins, the one-photon transition is made possible through hyperfine-induced mixing between the $2s2p\,^{1,3}P$ states, the so-called *hyperfine quenching* effect, and becomes the dominant decay mode of the $^3P_0$ state in very low density plasmas such as those found astrophysically.

Hyperfine quenching of the $2s2p\,^3P_0$ state in Be-like ions have been subject to theoretical and experimental investigations. On the theory side, hyperfine-induced decay rates of this state were calculated by Brage *et al.* [1] for a few low-Z ions of astrophysical interests in a perturbative approach using correlated wave functions obtained from the multiconfiguration Hartree-Fock (MCHF), the multiconfiguration Dirac-Fock (MCDF) and the F-dependent configuration-interaction (FCI) methods. The most extensive studies of these decay rates, however, were carried out earlier by Marques *et al.* [2] for the entire isoelectronic sequence in a complex matrix scheme, though their MCDF calculations gave an incomplete account of correlation effects.

Experimental determination of the hyperfine-induced decay rate of the $2s2p\,^3P_0$ state in Be-like ions are rather scarce. Only recently have two experimental results been reported. For $^{14}N^{3+}$, this rate was determined from observations of a planetary nebula [3]. The result of 4×10^{-4} s^{-1} is consistent with theory [1], though the uncertainty is rather high at 33%. More recently, the storage-ring measurement of the $^{47}Ti^{18+}$ ion gives a much more accurate hyperfine-induced decay rate of 0.56(3) s^{-1} [4]. However, this result is almost 60% larger then the sole theoretical prediction of 0.36 s^{-1} [2] and the difference was attributed to residual correlation effects in [4].

In spite of this seemingly large discrepancy between theory and experiment, it should be noted that results of the two existing calculations [1] and [2] readily differ by more than 60%. Besides differences in theoretical hyperfine quenching approaches and in correlation calculations, these two works also differ in the way the $2s2p^1P_1$ state is handled: It is excluded from the calculations of Marques *et al.* [2] who expected its contribution to the hyperfine quenching of the $2s2p\,^3P_0$ state to be negligible, but is included in the calculations of Brage

et al. [1] who came to just the oppose conclusion and showed that coherent mixing effects between the $2s2p\ ^{1,3}P_1$ states can be very important. In all, results of these two works can differ by more than a factor of three for low-Z Be-like ions. Before meaningful comparisons can be made with experiment, theoretical calculation should be scrutinized more closely.

In this work, we perform comprehensive calculations of the hyperfine-induced decay rates of the $2s2p\ ^3P_0$ state for Be-like ions with $Z = 6 - 92$. We use both the perturbative and the complex matrix approaches to shed light on the validity and limitation of these methods. We also use a radiation damping scheme for added theoretical insights. Special attention is given to the coherent hyperfine-mixing effects between the $2s2p\ ^{1,3}P_1$ states. To better account for electron correlation effects, a large-scale relativistic configuration-interaction (RCI) method [5–7] is used to calculate energy levels, radiative transition rates, and hyperfine matrix elements for the $2s^2\ ^1S_0$ and $2s2p\ ^{1,3}P_J$ states. While it is impractical to carry out these large-scale, time-consuming calculations for every Be-like ions, they are used for selected ions between $Z = 6$ and 92. Corresponding calculations are carried out with the much simpler MCDF method for every ions. Differences between RCI and MCDF results are then interpolated to provide correlation corrections to the MCDF results for every Be-like ions. This procedure gives results that are essentially the same as those from direct RCI calculations.

Since hyperfine quenching effects are sensitive to energy level spacings, we use empirical energies from the NIST Atomic Spectra Database [8] which are available for all four $2s2p$ states up to $Z = 29$. For higher Z ions, we use RCI energies which include mass polarization (MP) and quantum electrodynamic (QED) corrections. Both the magnetic dipole (M1) and electric quadrupole (E2) hyperfine interactions are included in the present hyperfine quenching calculations, though E2 contributions to the hyperfine-induced $^3P_0$ decay rates are found to be negligible and will not be presented here. In the following, we first describe our present calculations and review different theoretical approaches. We then show our results and compare them with other theories and with experiment.

II. THEORETICAL CALCULATIONS

A. Atomic structure

1. *Relativistic configuration-interaction method*

The energy level and transition diagram of the $2s^2$ and $2s2p$ states of Be-like ions are displayed in Fig. 1. Of the four $2s2p$ states, the $^{1,3}P_1$ states can decay to the ground state by E1 transitions (though the $^3P_1$ decay is spin-forbidden nonrelativistically), while the $^3P_2$ state decays by M2 transition. The $^3P_0$ state is forbidden to decay to the ground state by an one-photon transition except when it is induced by hyperfine interactions. This hyperfine-induced transition is sensitive to the fine-structure intervals of the $^{1,3}P$ states. In particular, since the $^3P_1$ state is the closest to the $^3P_0$ state along the isoelectronic sequence, it has the strongest influence on the hyperfine-induced decays of the latter.

For an accurate treatment of relativistic correlation effects, we use a relativistic configuration-interaction (RCI) method here. Details of our RCI method have been presented before [5, 6]. Briefly, our RCI method is based on the relativistic no-pair Hamiltonian [9, 10] which includes Coulomb and frequency-dependent, retarded Breit interactions. B-spline basis functions used here are solutions of the radial Dirac equation for an electron moving in a Dirac-Kohn-Sham (DKS) potential confined to a finite cavity [11]. The confinement in a cavity leads to discrete positive- and negative-energy states that form a set of finite, complete basis functions suitable for high-precision calculations.

Our RCI calculations start from the reference states $1s^22s^2 + 1s^22p^2$ and $1s^22s2p$ for the ground and excited states, respectively. RCI expansions include all possible single and double excitations from these reference states that arise from valence-valence, core-valence and core-core interactions. This procedure provides a systematic way of including all dominant configurations in RCI calculations for well converged results. We use only positive-energy B-spline orbitals with angular symmetry up to $l = 6$. Resulting RCI expansions have exceeded 200 000 configurations and the first few eigenstates of these large RCI matrices are obtained by an iterative Davidson's method [12] as implemented by Stathopoulos and Froese Fischer [13]. RCI eigenfunctions of the $2s^2\ ^1S_0$ and $2s2p\ ^{1,3}P_J$ states are then used to calculate transition rates and hyperfine matrix elements.

2. Mass polarization and QED corrections

In this work, empirical energies from the NIST Atomic Spectra Database [8] are used for $Z \leq 29$. At higher Z, RCI energies with mass polarization (MP) and quantum electrodynamic (QED) corrections are employed. Mass polarization corrections are calculated from first-order perturbation theory with the operator $(1/M)\sum_{i<j}\mathbf{p}_i \cdot \mathbf{p}_j$, where M is the nuclear mass, using eigenvectors from our RCI calculations. QED corrections consist of self-energy and vacuum polarization corrections, both calculated in the same DKS potential as in the RCI calculations to account for screening effects. Specifically, one-electron self-energies are calculated non-perturbatively to all orders of $Z\alpha$ in DKS potentials with partial wave expansions in the configuration space using numerical bound-state Green's functions. Subtraction terms involving the free-electron propagator are evaluated in momentum space with Fourier-transformed wave functions. Details of these self-energy calculations, with references to earlier works, can be found in Ref. [14]. As for vacuum polarizations, leading contributions are obtained from expectation values of the Uehling potential, while higher-order Wichmann-Kroll corrections, like electron self-energies, are calculated non-perturbatively in DKS potentials with partial wave expansions in the configuration space using numerical bound-state Green's functions [15]. Total QED corrections are given by sums of one-electron QED contributions, weighted by the generalized occupation numbers of each electrons. Theoretical RCI energies including the MP and QED corrections have been found to be in excellent agreement with empirical energies for the $2s2p\,{}^{1,3}P_1$ states before [5, 6] and should be reliable for all four $2s2p$ states here.

3. Radiative transitions

The electric-dipole (E1) and magnetic quadruple (M2) radiative transition matrix elements are calculated from first-order perturbation theory using the frequency-dependent electromagnetic multipole transition operators $Q_k^{(\lambda)}$, where k is the multipole order and $\lambda = 1/0$ for electric/magnetic multipoles. Explicit formulas of $Q_k^{(\lambda)}$ (in length and velocity gauges for electric multipoles) are given in Ref. [16]. In particular, for E1 transitions in the length gauge, $Q_1^{(1)}$ reduces to the dipole operator $\mathbf{D} = \sum_i -e\mathbf{r}_i$ in the nonrelativistic limit. Defining $Q_1 = Q_1^{(1)}/ea_0$ and $M_2 = Q_2^{(0)}/\mu_{\rm B}a_0$ as the dimensionless electric dipole and

magnetic quadrupole transition operators, respectively, with a_0 being the Bohr radius and $\mu_{\rm B} = e\hbar/2mc$ the Bohr magneton, then $Q_1 = Q_1^{(1)}$ and $M_2 = 2cQ_2^{(0)}$ in a.u., and E1 and M2 decay rates from an initial state $|i\rangle$ to a final state $|f\rangle$ are given by

$$A_{\rm E1}(i \to f) = \frac{2.02613\times10^{18}}{\lambda^3} \frac{|\langle i\|Q_1\|f\rangle|^2}{(2J_i+1)}, \tag{1}$$

$$A_{\rm M2}(i \to f) = \frac{1.49097\times10^{13}}{\lambda^5} \frac{|\langle i\|M_2\|f\rangle|^2}{(2J_i+1)}, \tag{2}$$

where $A_{\rm E1}$ and $A_{\rm M2}$ are in $\rm s^{-1}$, the transition wavelength λ is in Å, and transition matrix elements are dimensionless.

The computational procedure of our RCI transition calculations can be found in [7]. Briefly, many-electron transition matrix elements are reduced into sums of one-electron radial transition matrix elements weighted by configuration mixing coefficients and angular recoupling factors using a computer code which is based on the MCT package in the Oxford MCDF program [17]. Formulas for the radial transition matrix elements are given in [16]. It should be noted that since negative-energy states are excluded from our *no-pair* calculations, resulting E1 transition rates are intrinsically gauge dependent, especially for the spin-forbidden $2s2p\,^3P_1 - 2s^2\,^1S_0$ intercombination transition where length and velocity gauge results can differ by a factor two in low-Z Be-like ions [7]. However, as shown in [7], E1 transition matrix elements calculated in the length gauge are insensitive to contributions from negative-energy states and the length gauge is what we use for E1 calculations here. There is no gauge issue with magnetic multipole transitions.

B. Hyperfine interaction

The relativistic hyperfine interaction Hamiltonian can be written as [18, 19]

$$H_{\rm HF} = \sum_k \mathbf{M}^{(k)} \cdot \mathbf{T}^{(k)}, \tag{3}$$

where $\mathbf{M}^{(k)}$ and $\mathbf{T}^{(k)}$ are spherical tensor operators of rank k representing the nuclear and electronic parts, respectively, of the hyperfine interaction. The hyperfine state $|IJFM_F\rangle$ is formed by coupling the nuclear state $|IM_I\rangle$ and the atomic state $|JM_J\rangle$ to give an eigenstate of the total angular momentum $\mathbf{F} = \mathbf{I} + \mathbf{J}$, where $\mathbf{I}$ and $\mathbf{J}$ are the nuclear spin and the total

angular momentum of the atomic state, respectively, such that

$$|IJFM_F\rangle = \sum_{M_I M_J} \langle IM_I JM_J|FM_F\rangle \, |IM_I\rangle|JM_J\rangle \, . \tag{4}$$

The matrix element of the hyperfine operator is then given by [18, 19]

$$\begin{aligned} W_{JJ'} &= \langle IJFM_F| \sum_k \mathbf{M}^{(k)} \cdot \mathbf{T}^{(k)} |IJ'FM_F\rangle \\ &= \sum_k (-1)^{I+J+F} \left\{ \begin{array}{ccc} I & J & F \\ J' & I & k \end{array} \right\} \langle I\|M^{(k)}\|I\rangle \, \langle J\|T^{(k)}\|J'\rangle \, . \end{aligned} \tag{5}$$

For the magnetic dipole (M1) hyperfine interaction, $k = 1$ and the nuclear magnetic moment μ_I, in units of the nuclear magneton $\mu_N = e\hbar/2m_p c$, is defined by the nuclear *stretched* state $|I\, M_I{=}I\rangle$ as

$$\mu_I \mu_N = g_I I \mu_N = \langle II|M^{(1)}|II\rangle = \frac{I}{\sqrt{I(I+1)(2I+1)}} \, \langle I\|M^{(1)}\|I\rangle \, . \tag{6}$$

The magnetic dipole hyperfine operator $T^{(1)}_q$ is given by [18]

$$T^{(1)}_q = \sum_j -ie \sqrt{\frac{8\pi}{3}} \, r_j^{-2} \, \boldsymbol{\alpha}_j \cdot \mathbf{Y}^{(0)}_{1q}(\hat{\mathbf{r}}_j) \, , \tag{7}$$

in which $\boldsymbol{\alpha}$ is the Dirac matrix and $\mathbf{Y}^{(\lambda)}_{kq}(\hat{\mathbf{r}})$ represents the vector spherical harmonics [20]. The sum here is over all electrons in the atom, though there are no net contributions from closed shells. In this work, Gaussian units where $1/4\pi\epsilon_0 = 1$ are used. In particular, the sign of e is significant and $e = |e|$ is the magnitude of the electron charge here. From Eqs. (5) and (6), M1 hyperfine energies are given by

$$W^{\rm M1}_{JJ'} = \mu_N \left(\frac{\mu_I}{I}\right) (-1)^{I+J+F} \sqrt{I(I+1)(2I+1)} \left\{ \begin{array}{ccc} I & J & F \\ J' & I & 1 \end{array} \right\} \langle J\|T^{(1)}\|J'\rangle \, , \tag{8}$$

where $W^{\rm M1}_{JJ'}$ is in a.u. if $\mu_N = 1.987131 \times 10^{-6}$ and in MHz if $\mu_N = 13074.70$, and $\langle J\|T^{(1)}\|J'\rangle$ is in a.u.. For isolated atomic states, M1 hyperfine energies are basically determined by the diagonal matrix element $W^{\rm M1}_{JJ}$ in terms of the hyperfine constant A_J as

$$W^{\rm M1}_{JJ} = A_J K/2 \, , \tag{9}$$

where

$$A_J = \mu_N \left(\frac{\mu_I}{I}\right) \frac{\langle J\|T^{(1)}\|J\rangle}{\sqrt{J(J+1)(2J+1)}} \, , \tag{10}$$

and $K = F(F+1) - I(I+1) - J(J+1)$.

The reduction of the many-electron hyperfine matrix elements $\langle J \| T^{(k)} \| J' \rangle$ into sums of one-electron radial matrix elements weighted by configuration mixing coefficients and angular recoupling factors follows the same angular recoupling procedure as in the case of radiative transitions. In fact, as angular selection rules for the hyperfine matrix elements are the same as those for the corresponding electromagnetic multipole transitions, we can utilize our RCI radiative transition codes for hyperfine interaction calculations by simply replacing the transition radial matrix elements with hyperfine radial matrix elements. Formulas for the latter can be found in [18].

As for the electric quadrupole (E2) hyperfine interactions, they can be calculated in a similar fashion, with formulas for the nuclear quadrupole moment Q and the E2 hyperfine operator $T^{(2)}_q$ readily given in [18]. However, as their contributions to the hyperfine-induced decay of the $^3P_0$ state are found to be completely negligible, E2 hyperfine interactions will not be considered here.

C. Hyperfine-induced transition rates

The hyperfine Hamiltonian is given by

$$H = H_0 + H_{\rm HF}\,, \tag{11}$$

where H_0 is the relativistic no-pair Hamiltonian and $H_{\rm HF}$ is the hyperfine interaction Hamiltonian shown in Eq. (3). For hyperfine quenching calculations, the starting point is the determination of atomic eigenstates $|\gamma JM\rangle$ of the no-pair Hamiltonian, here with the RCI method, such that

$$H_0\,|\gamma_i\,J_i\,M_i\rangle = E_i\,|\gamma_i\,J_i\,M_i\rangle\,. \tag{12}$$

For brevity, the atomic-state identification quantum number γ_i will be dropped when possible and the five $n = 2$ atomic states will be identified by the subscript i such that $i = 0$, 1, 2, 3, 4 for the $2s^2\,{}^1S_0$, $2s2p\,{}^3P_{0,1,2}$ and $2s2p\,{}^1P_1$ states, respectively. Several approaches have been used to study the hyperfine-induced transition rates. We shall briefly describe them in the following.

1. The perturbative approach

The perturbative approach was used by Johnson *et al.* for hyperfine quenching studies of He-like ions [19] and by Brage *et al.* for Be-like ions [1]. In this approach, hyperfine eigenstates are first determined from the Hamiltonian $H_0 + H_{\rm HF}$ and radiative transitions between them are then calculated from perturbation theory. For the $2s^2\,{}^1S_0$ ground state, the hyperfine eigenstate is simply given by $|{}^1S_0\,FM\rangle = |IJ_0\,FM\rangle$ with $J_0 = 0$ and $F = I$. For the $2s2p\,{}^{1,3}P$ states, they are given by

$$|\gamma_j FM\rangle = \sum_{i=1}^{4} c_i^{(j)} |IJ_i FM\rangle\,, \quad j = 1-4\,, \tag{13}$$

where the mixing coefficients $c_i^{(j)}$ are determined by diagonalizing the hyperfine matrix

$$\begin{pmatrix} 0 & W_{12} & W_{13} & W_{14} \\ W_{21} & \Delta E_{21} + W_{22} & W_{23} & W_{24} \\ W_{31} & W_{32} & \Delta E_{31} + W_{33} & W_{34} \\ W_{41} & W_{42} & W_{43} & \Delta E_{41} + W_{44} \end{pmatrix}, \tag{14}$$

with $\Delta E_{ij} = E_i - E_j$ being the fine structure intervals and $W_{ij} = \langle IJ_iFM|H_{\rm HF}|IJ_jFM\rangle \approx W_{ij}^{\rm M1}$ the hyperfine energies. For the $2s2p\,{}^3P_0$ state, there is only one $F = I$ hyperfine level, hence only one $F = I$ hyperfine matrix to deal with, and the hyperfine-induced (HFI) decay rate is given by [19]

$$\begin{aligned} A_{\rm HFI}({}^3P_0) \;=\; & \frac{6.75376\times10^{17}}{\lambda_1^3}\,\left|\, c_2\langle {}^1S_0\|Q_1\|{}^3P_1\rangle + c_4\langle {}^1S_0\|Q_1\|{}^1P_1\rangle\right|^2 \\ & + \frac{2.98194\times10^{12}}{\lambda_1^5}\,\left|\, c_3\langle {}^1S_0\|M_2\|{}^3P_2\rangle\right|^2, \end{aligned} \tag{15}$$

where $A_{\rm HFI}$ is in $\rm s^{-1}$, λ_1 is the transition wavelength between the ${}^3P_0$ and ${}^1S_0$ states in Å, $c_i = c_i^{(1)}$ are the configuration mixing coefficients for the ${}^3P_0$ hyperfine state, and Q_1 and M_2 are the E1 and M2 transition operators shown in Eqs. (1) and (2).

In general, $A_{\rm HFI}({}^3P_0)$ is dominated by contributions from the ${}^3P_1$ state which is the closest to, and has the strongest hyperfine mixing with, the ${}^3P_0$ state, and is readily given by

$$A_{\rm HFI}({}^3P_0) \;\approx\; c_2^2\,\tilde{A}_2 \;=\; c_2^2\,\tilde{A}_{\rm E1}({}^3P_1)\,, \tag{16}$$

where $\tilde{A}_{\rm E1}({}^3P_1) = (\lambda_2/\lambda_1)^3 A_{\rm E1}({}^3P_1)$ is the energy-scaled decay rate and λ_i is the transition wavelength from state i to the ${}^1S_0$ ground state. However, contributions from the ${}^1P_1$ state

can be significant due to the coherent mixing between the $^1P_1$ and $^3P_1$ states shown in Eq. (15), especially at low Z where the $^1P_1 - {}^1S_0$ transitions are much stronger then the $^3P_1 - {}^1S_0$ spin-forbidden transitions. Contributions from the M2 transition to $A_{\rm HFI}$, on the other hand, is found to be quite negligible and, for all practical purposes, the last term in Eq. (15) can be omitted.

2. The complex matrix method

The complex matrix method was first used by Indelicato *et al.* for hyperfine quenching studies of He-like ions [21] and later by Marques *et al.* for Be-like ions [2]. In this approach, radiative half-widths of the fine structure levels are added as imaginary parts to the diagonal matrix elements of the hyperfine matrix, shown in Eq. (14), such that

$$H_{jk} = (\Delta E_{j1} + i\Gamma_j/2)\delta_{jk} + W_{jk}\,, \tag{17}$$

with $\Gamma_j = \hbar A_j$ being the radiative line width, and A_j the decay rate, of state j. Diagonalization of this matrix leads to complex eigenenergies, the real parts of which are the hyperfine energy levels, and the imaginary parts the hyperfine half-widths from which the quenching rates are determined. Indelicato *et al.* [21] and Marques *et al.* [2] further considered only hyperfine mixing between the $^3P_0$ and $^3P_1$ states, resulting in a 2×2 eigenvalue problem

$$\begin{pmatrix} 0 & W_{12} \\ W_{21} & \Delta E_{21} + W_{22} + i\Gamma_2/2 \end{pmatrix} \tag{18}$$

involving only 4 parameters: the fine structure splitting ΔE_{21}, the hyperfine energies W_{12} and W_{22}, and the decay rate A_2.

The complex matrix method is a nonperturbative method in which the radiation field is treated on the same footing as the hyperfine interaction instead of perturbatively after the hyperfine states are determined. It can handle cases where the radiative half-width $\Gamma_2/2$ of the $^3P_1$ state is comparable in size to the level spacing ΔE_{21} between the $^3P_0$ and $^3P_1$ states, a situation not suitable for the perturbative approach. This happens to the hyperfine quenching of the $1s2p\,{}^3P_0$ state in He-like ions with $Z > 40$ where the decay rate A_2, hence the half-width $\Gamma_2/2$, of the $1s2p^3P_1$ state is greatly enhanced by the large $n = 2-1$ transition energy. However, the lack of coherent hyperfine mixing between the $^1P_1$ and $^3P_1$ states renders the complex matrix method unsuitable for low-Z He-like ions even if the full

4×4 complex matrix is used. Thus, the complex matrix method is seen to compliment the perturbative approach for treating hyperfine quenching in He-like ions, with the latter works at low Z while the former works at high Z [19].

Such is not the case for Be-like ions here. To begin with, as the half-width $\Gamma_2/2$ from the $n = 2 - 2$ transitions is consistently small compared to the fine structure splitting ΔE_{21}, the perturbative approach should work along the entire isoelectronic sequence. More importantly, while the complex matrix method is still not expected to work at low Z due to the lack of coherent hyperfine mixing between the $^{1,3}P_1$ states, its validity at high Z is no longer certain. Indeed, from the above 2×2 matrix, when Γ_2 is small, the hyperfine-induced decay rate is readily given by

$$A_{\rm HFI}(^3P_0) \approx c_2^2\, A_2 = c_2^2 A_{\rm E1}(^3P_1)\,. \tag{19}$$

Comparing with Eq. (16) from the perturbative approach under the same approximation, the two induced rates are seen to be different by the energy scaling factor $(\lambda_2/\lambda_1)^3$. The lack of this factor is a problem for the complex matrix method, as it comes from the phase space factor of the hyperfine-induced $^3P_0 - {}^1S_0$ transition with the induced wavelength $\lambda \approx \lambda_1$ mandated by energy conservation. For He-like ions, this problem can be overlooked as $\lambda_1 \approx \lambda_2$ for the $n = 2-1$ transitions. For the $n = 2-2$ transitions in Be-like ions, however, the difference between λ_1 and λ_2 is usually not negligible and complex matrix results will be different from perturbative results even for high-Z ions.

3. The radiation-damping method

The radiation-damping method is another nonperturbative scheme in which the radiation field and the hyperfine interaction are treated on the same footing. It was introduced by Johnson *et al.* [19] to study hyperfine quenching in He-like ions. In this approach, interactions with the radiation field are included by means of a nonlocal optical potential $V_{\rm rd}$ used by Robicheaux *et al.* [22] to treat radiation damping in scattering states. Specifically, $V_{\rm rd}$ is defined by its action on an eigenstate $|\Psi_E\rangle$ with energy E such that

$$V_{\rm rd}\,|\Psi_E\rangle = i \sum_{kq\lambda} \frac{(k+1)(2k+1)}{k[(2k+1)!!]^2} \sum_n \left(\frac{\omega_n}{c}\right)^{2k+1} Q^{(\lambda)}_{kq}\,|n\rangle\,\langle n|\,Q^{(\lambda)\dagger}_{kq}\,|\Psi_E\rangle\,, \tag{20}$$

where $Q^{(\lambda)}_{kq}$ is the multipole transition operator presented in Section II A 3, $|n\rangle$ are atomic states lower in energy than $|\Psi_E\rangle$, and $\omega_n = (E - E_n)/\hbar$.

The potential $V_{\rm rd}$ is a spherically symmetric, anti-Hermitian operator and its matrix elements are nonvanishing only between states of the same angular momentum. For the $^3P_0$ hyperfine eigenstate defined in Eq. (13), the only state $|n\rangle$ lower in energy is the $^1S_0$ ground state and there are four nonvanishing matrix elements for $V_{\rm rd}$ between the four $2s2p$ basis states as given by Eqs. (2.19) - (2.22) in Ref. [19]. The first three are diagonal matrix elements

$$\langle\, ^3P_1 \,|\, V_{\rm rd} \,|\, ^3P_1 \rangle \;=\; i\tilde{\Gamma}_2/2 \;=\; i\hbar\tilde{A}_2/2\,, \tag{21}$$

$$\langle\, ^3P_2 \,|\, V_{\rm rd} \,|\, ^3P_2 \rangle \;=\; i\tilde{\Gamma}_3/2 \;=\; i\hbar\tilde{A}_3/2\,, \tag{22}$$

$$\langle\, ^1P_1 \,|\, V_{\rm rd} \,|\, ^1P_1 \rangle \;=\; i\tilde{\Gamma}_4/2 \;=\; i\hbar\tilde{A}_4/2\,, \tag{23}$$

while the fourth is the off-diagonal matrix element

$$\langle\, ^3P_1 \,|\, V_{\rm rd} \,|\, ^1P_1 \rangle = (i/2)\,\rho\,\sqrt{\tilde{\Gamma}_2\,\tilde{\Gamma}_4} \;=\; (i/2)\,\rho\,\hbar\,\sqrt{\tilde{A}_2\,\tilde{A}_4}\,, \tag{24}$$

where $\tilde{A}_2 = A_{\rm E1}(^3P_1)(\lambda_2/\lambda_1)^3$, $\tilde{A}_3 = A_{\rm M2}(^3P_2)(\lambda_3/\lambda_1)^5$, and $\tilde{A}_4 = A_{\rm E1}(^1P_1)(\lambda_4/\lambda_1)^3$ are the energy-scaled decay rates, and ρ is the sign of $\langle\, ^1S_0 \,\|\, Q_1 \,\|\, ^3P_1\rangle\langle\, ^1S_0 \,\|\, Q_1 \,\|\, ^1P_1\rangle$. Energy scaling factors $(\lambda_i/\lambda_1)^m$, $m = 3$ or 5 for E1 or M2 transition, show up here because the transition frequency ω_n in Eq. (20) is specific to the eigenstate $|\Psi_E\rangle$. If the hyperfine eigenstate in question is the $^3P_1$ instead of the $^3P_0$ state, the four matrix elements of $V_{\rm rd}$ will still be given by the above equations, but the energy scaling factors will be changed to $(\lambda_i/\lambda_2)^m$.

Like the complex matrix approach, including $V_{\rm rd}$ together with $H_0 + H_{\rm HF}$ leads to a complex generalization of the 4×4 hyperfine matrix such that the real and imaginary parts of the eigenvalues give the energies and half-widths of the hyperfine levels, respectively. This nonperturbative treatment of the radiation field should make the radiation damping method work for high-Z ions. Unlike the complex matrix method, however, the imaginary parts of the diagonal matrix elements consist of the *state-specific*, energy-scaled half-widths instead of the actual radiative half-widths of the $2s2p$ states. Furthermore, with the addition of the imaginary non-diagonal matrix element shown in Eq. (24), coherent mixing between the $^3P_1$ and $^1P_1$ states is correctly accounted for. Both of the these features are consistent with those in the perturbative approach and make the radiation damping method work for low-Z ions also. Indeed, the radiation damping method has been shown to work for all He-like ions, with results reducing to perturbative results for $Z < 40$ and to complex matrix results for higher Z ions [19]. It is expected to work for all Be-like ions also.

III. RESULTS AND DISCUSSION

In this work, atomic structure data are calculated with the RCI method. These large-scale calculations are computer intensive and it is not practical to carry them out for every Be-like ion. Instead, they are used for fifteen ions with Z = 6, 7, 10, 13, 18, 22, 32, 38, 45, 55, 64, 76, 83, 88 and 92. Much simpler MCDF calculations are carried out for every ion between $Z = 6 - 92$ in the extended average level (EAL) scheme [17] with $2s^2 + 2p^2$ configurations for the ground state and $2s2p$ configurations for the excited states. Differences between the RCI and MCDF results on energy levels, transition line strengths, hyperfine matrix elements and mass polarization corrections are interpolated to provide correlation corrections to the MCDF results for every Be-like ion. Atomic structure data obtained this way are found to be just as accurate as those from direct RCI calculations and will be referred to as RCI results in the following. As for QED energies, they are calculated for ten ions with Z = 26, 32, 38, 45, 55, 64, 76, 83, 88 and 92 and are interpolated to every ion between $Z = 26 - 92$ assuming a $(Z\alpha)^4$ dependence. This procedure should give accurate enough results for these small corrections.

In Table I, energy levels of the $2s2p\ ^{1,3}P_J$ states relative to the $2s^2\ ^1S_0$ ground states are shown. For $Z = 6 - 29$, results are from the NIST Atomic Spectra Database [8]. For higher-Z ions, they are from the present RCI calculations and include mass polarization and QED corrections. Contributions to theoretical energies for selected Be-like ions with $Z \geq 26$ are shown in Table II and are compared with available empirical energies. It can be seen that the present RCI energies agree with experiment to better than 0.1% in all cases. This is consistent with our earlier finding that RCI energies of the $^{1,3}P_1$ states are in good agreement with experiment throughout the isoelectronic sequence [5, 6].

In Table III, the unperturbed radiative decay rates from the $^{1,3}P_1$ and $^3P_2$ states to the $^1S_0$ ground state are shown for $Z = 6 - 92$. These rates are calculated with transition energies from Table I and E1 rates are calculated in the length gauge. Comparisons with other theories and with experiment for the $^{1,3}P_1$ E1 decay rates are shown in Table IV. In general, there are good agreement between theories and experiments, especially for the $^1P_1$ decay rates. At Z = 6, the spin-forbidden $^3P_1$ decay rate of 79.5 s^{-1} by Marques *et al.* [2] is smaller than the measured value of 103 s^{-1} [23] by about 20% due to an inadequate treatment of electron correlations. However, the rather large discrepancy in the $^3P_1$ decay

rate at $Z = 42$ between the present RCI and the MCDF calculations of Ynnerman and Froese Fischer [24] is not due to differences in correlation calculations but to the neglect of QED corrections in [24] which, as shown in Table II, amount to a 3% correction in the transition energy and would change the $^3P_1$ decay rate in [24] from 9.37×10^8 s^{-1} to 8.64×10^8 s^{-1}, in perfect agreement with the present result of 8.65×10^8 s^{-1}.

In Table V, M1 hyperfine reduced matrix elements between the ^3P_J states are shown. Similar results between the $^1P_1$ and $^{1,3}P_J$ states are given in Table VI. E2 hyperfine reduced matrix elements have also been calculated, but as their contributions to hyperfine intervals in general, and to hyperfine quenching of the $^3P_0$ state in particular, are found to be quite small, they will not be presented here. With results from Tables I, V and VI, hyperfine intervals of the $^{1,3}P$ states can easily be calculated from Eq. (14). In particular, first-order hyperfine intervals are readily given by the diagonal hyperfine matrix elements in terms of the A_J coefficients from Eqs. (9) and (10). We note that the hyperfine energies W_{12} and W_{22} as computed from the matrix elements $\langle ^3P_0\|T^{(1)}\|^3P_1\rangle$ and $\langle ^3P_1\|T^{(1)}\|^3P_1\rangle$, respectively, are consistent in size with those by Marques *et al.* [2], but the sign of W_{22} is different between our two calculations. While signs of off-diagonal hyperfine matrix elements are some what arbitrary, signs of diagonal hyperfine matrix elements are very specific, as they affect the ordering of hyperfine levels. The sign difference observed here has also been noted by Johnson *et al.* [19] when comparing their RCI results with the MCDF results of Indelicato *et al.* [21] on the hyperfine quenching of He-like ions. It is quite likely that the sign error in [21] has persisted in [2].

In Table VII, the hyperfine-induced decay rates for the $^3P_0$ state are shown for stable isotopes of Be-like ions with $6 \le Z \le 92$. Nuclear magnetic moments μ_I are from the tabulation by Raghavan [25]. These rates are calculated from the perturbative approach with the full 4×4 hyperfine matrix and include coherent mixing contributions from the $^1P_1$ state. Unlike He-like ions where the perturbative approach only works for $Z < 40$ [19], it works for all Be-like ions here, as radiative linewidths of the $2s2p$ states are consistently small compare to the level spacings. This is confirmed by our radiative damping results which are indistinguishable from the perturbative results along the entire isoelectronic sequence.

Because of the dependence on the nuclear spin I and nuclear magnetic moment μ_I, it is difficult to establish systematic trends for these induced rates. However, Brage *et al.* [1] have shown that the scaled hyperfine-induced decay rate $\tilde{A}_{\rm HFI}$ for the $^3P_0$ state as defined

by

$$\tilde{A}_{\rm HFI}(^3P_0) = A_{\rm HFI}(^3P_0) \,/\, [\mu^2(1+1/I)] \tag{25}$$

is relatively independent of nuclear effects. Indeed, we find that $\tilde{A}_{\rm HFI}$ as calculated from different isotopes of the same atom agree to better than 1% for all Be-like ions. In Table VIII, the scaled hyperfine-induced decay rates for the $^3P_0$ state are compared between theory and experiment for selected Be-like ions. Some of these comparisons are also shown in Fig. 2 along the isoelectronic sequence. Here, the 2×2 matrix results include hyperfine mixing between the $2s2p\ ^3P_0$ and $^3P_1$ states only, while the 4×4 matrix results include hyperfine mixing between all four $2s2p$ states. For brevity, we use PT and CM to stand for perturbative and complex matrix results, respectively. Radiation damping results are identical to the corresponding perturbative results and will not be mentioned.

For low-Z ions, the 2×2 results are substantially smaller than the 4×4 results. Indeed, at $Z = 6$, our PT-2×2 RCI value of 2.13×10^{-4} s^{-1} is only about 40% of our PT-4×4 RCI value of 5.56×10^{-4} s^{-1}. This shows the importance of including the $^1P_1$ state at low Z, as the $^1P_1 - {}^1S_0$ transition is much stronger than the $^3P_1 - {}^1S_0$ intercombination transition in the LS-coupling limit. As Z increases, contributions from the $^1P_1$ state steadily decease and the two results can be seen to approach each other in Fig. 2. This is due in part to the widening of the energy separation ΔE_{41} between the $^3P_0$ and $^1P_1$ states relative to ΔE_{21} between the $^3P_0$ and $^3P_1$ states as depicted in Fig. 1, and in part to the rapid increase in the intercombination decay rate A_1 of the $^3P_1$ state toward the jj-coupling limit. It can also be seen in Table VIII and Fig. 2 that the present PT-2×2 and PT-4×4 RCI results are in good agreement with corresponding perturbative results of Brage *et al.* [1] as calculated with correlated MCHF, MCDF and FCI methods.

As for the complex matrix scheme, 2×2 results also differ from 4×4 results at low Z but agree at high Z. At $Z = 6$, our CM-2×2 RCI complex matrix value of 2.13×10^{-4} s^{-1} is the same as our PT-2×2 RCI value, while the CM-2×2 MCDF result of Marques *et al.* is lower at 1.55×10^{-4} s^{-1} due to their inadequate treatments of correlation effects. When contributions from the $^1P_1$ state are added incoherently, our CM-4×4 RCI value jumps to 8.14×10^{-4} s^{-1}, but coherent mixing between the $^{1,3}P_1$ states brings our PT-4×4 RCI value back down to 5.56×10^{-4} s^{-1}. These changing results clearly demonstrate the importance of electron correlations and coherent hyperfine mixing to the hyperfine-induced decay rates of low-Z ions. Furthermore, while our CM-2×2 and CM-4×4 RCI results agree at high Z,

their values are different from the perturbative ones even though correlation effects are no longer important. This is due to the energy scaling factor $(\lambda_2/\lambda_1)^3$ which shows up in Eq. (16) of the perturbative approach and in Eq. (22) of the radiation damping method but not in Eq. (19) of the complex matrix scheme. For low-Z ions, as $^3P_0$ and $^3P_1$ states are nearly degenerate in energy, this energy scaling factor is close to one, and our CM-2×2 and PT-2×2 RCI results are almost the same. As Z increases, however, this factor steadily increases to 1.54 at $Z = 92$ and leads to a 54% difference between these two hyperfine-induced decay rates. The lack of coherent hyperfine mixing and *state-specific* energy scaling factors renders the complex matrix approach unsuitable for hyperfine quenching studies of Be-like ions here, and most likely for other alkaline-earth-like ions also.

As we have mentioned earlier, there are only two empirical data available for the hyperfine-induced $^3P_0$ decay rates to date. For $^{14}N^{3+}$, the empirical value of 4×10^{-4} s^{-1} as deduced from observations of a planetary nebula with an estimated error of about 33% [3] is consistent with the perturbative results of this work and of Ref. [1]. As for $^{47}Ti^{18+}$, the value of 0.56(3) s^{-1} from the recent storage ring measurement [4] is higher than the 2×2 complex matrix result of 0.36 s^{-1} by Marques *et al.* [2] by almost 60%. Our present 4×4 RCI perturbative result of 0.67 s^{-1} is closer to, but 20% higher than, the measured value.

In summary, accurate energy levels and decay rates of the $2s2p\,^{1,3}P_J$ states are determined for all Be-like ions from $Z = 6 - 92$ using the RCI method here. Hyperfine matrix elements between these $2s2p$ states are also calculated and can be used to determine their hyperfine energy levels. In particular, hyperfine-induced decay rates of the $2s2p\,^3P_0$ state are calculated using the perturbative, the complex matrix and the radiation damping approaches. Perturbative and radiation damping results are found to agree with each other for all Be-like ions. Complex matrix results, on the other hand, consistently differ from the other two results and may not be reliable here. The present perturbative results are in good agreement with those by Brage *et al.* [1] for low- to mid-Z ions. Theoretical uncertainties from residual correlation corrections are likely to be no more than a few percent as measured by the small discrepancies between these two highly correlated calculations and are not expect to account for the remaining 20% discrepancy between theory and experiment for $^{47}Ti^{18+}$. More high-precision hyperfine quenching experiments for Be-like and other alkaline-earth-like ions will definitely be welcomed.

Acknowledgments

The work of K.T.C. and M.H.C was performed under the auspices of the U.S. Department of Energy by Lawrence Livermore National Laboratory under Contract DE-AC52-07NA27344. The work of W.R.J. was supported in part by NSF Grant No. PHY-0456828.

---

[1] T. Brage, P. G. Judge, A. Aboussaïd, M. R. Godefroid, P. Jönsson, A. Ynnerman, C. Froese Fisher, and D. S. Leckrone, Astrophy. J. **500**, 507 (1998).

[2] J. P. Marques, F. Parente, and P. indelicato, Phys. Rev. A **47**, 929 (1993).

[3] T. Brage, P. G. Judge, and C. R. Proffitt, Phys. Rev. Lett. **89**, 281101 (2002).

[4] S. Schippers, E. W. Schmidt, D. Bernhardt, D. Yu, A. Muller, M. Lestinsky, D. A. Orlov, M. Grieser, R. Repnow, and A. Wolf, Phys. Rev. Lett. **98**, 033001 (2007).

[5] M. H. Chen and K. T. Cheng, Phys. Rev. A **55**, 166 (1997).

[6] K. T. Cheng, M. H. Chen, and J. Sapirstein, Phys. Rev. A **62**, 054501 (2000).

[7] M. H. Chen, K. T. Cheng, and W. R. Johnson, Phys. Rev. A **64**, 042507 (2001).

[8] NIST Atomic Spectra Database, http://physics.nist.gov/PhysRefData/ASD.

[9] J. Sucher, Phys. Rev. A **22**, 348 (1980).

[10] M. H. Mittleman, Phys. Rev. A **4**, 893 (1971); **5**, 2395 (1972); **24**, 1167 (1981).

[11] W. R. Johnson, S. A. Blundell, and J. Sapirstein, Phys. Rev. A **37**, 307 (1988).

[12] E. R. Davidson, J. Comp. Phys. **17**, 87 (1975).

[13] A. Stathopulos and C. Froese Fischer, Comput. Phys. Comm. **79**, 268 (1994).

[14] J. Sapirstein and K. T. Cheng, Phys. Rev. A **73**, 012503 (2006).

[15] J. Sapirstein and K. T. Cheng, Phys. Rev. A **68**, 042111 (2003).

[16] W. R. Johnson, D. R. Plante, and J. Sapirstein, in *Advances in Atomic, Molecular, and Optical Physics*, edited by B. Bederson and H. Walther (Academic Press, San Diego, 1995), P. 251.

[17] I. P. Grant, B. J. McKenzie, P. H. Norrington, D. F. Mayers, and N. C. Pyper, Comput. Phys. Comm. **21**, 207 (1980).

[18] K. T. Cheng and W. J. Childs, Phys. Rev. A **31**, 2775 (1985).

[19] W. R. Johnson, K. T. Cheng and D. R. Plante, Phys. Rev. A **55**, 2828 (1997).

[20] A. J. Akhiezer and V. B. Berestetskii, *Quantum Electrodynamics* (Interscience, New York,

1965), Chap. 1, Sec. 4.2.

[21] P. indelicato, F. Parente, and R. Marrus, Phys. Rev. A **40**, 3505 (1989).

[22] F. Robicheaux, T. W. Gorczyca, M. S. Pindzola, and N. R. Badnell, Phys. Rev. A **52**, 1319 (1995).

[23] J. Doerfert, E. Träbert, A. Wolf, D. Schwalm, and O. Uwira, Phys. Rev. Lett. **78**, 4355 (1997).

[24] A. Ynnerman and C. Froese Fischer, Phys. Rev. A **51**, 2020 (1995).

[25] P. Raghavan, At. Data Nucl. Data Tables **42**, 189 (1989).

[26] P. Beiersdorfer, A. Osterheld, S. R. Elliott, M. H. Chen, D. Knapp, and K. Reed, Phys. Rev. A **52**, 2693 (1995).

[27] P. Beiersdorfer, D. Knapp, R. E. Marrs, S. R. Elliot, and M. H. Chen, Phys. Rev. Lett. **71**, 3939 (1993); P. Beiersdorfer, Nucl. Instru. and Methods in Phys. Research B **99**, 114 (1995).

[28] J. Fleming, A. Hibbert, and R. P. Stafford, Phys. Scr. **49**, 316 (1994).

[29] N. Reistad and I. Martinson, Phys. Rev. A **34**, 2632 (1986).

[30] E. Träbert, Z. Phys. D **9**, 143 (1988).

[31] L. Engström *et al.*, Phys. Scr. **24**, 551 (1981).

[32] E. Träbert and P. H. Heckmann, Phys. Scr. **22**, 489 (1980).

[33] J. B. Buchet *et al.*, Phys. Rev. A **30**, 309 (1984).

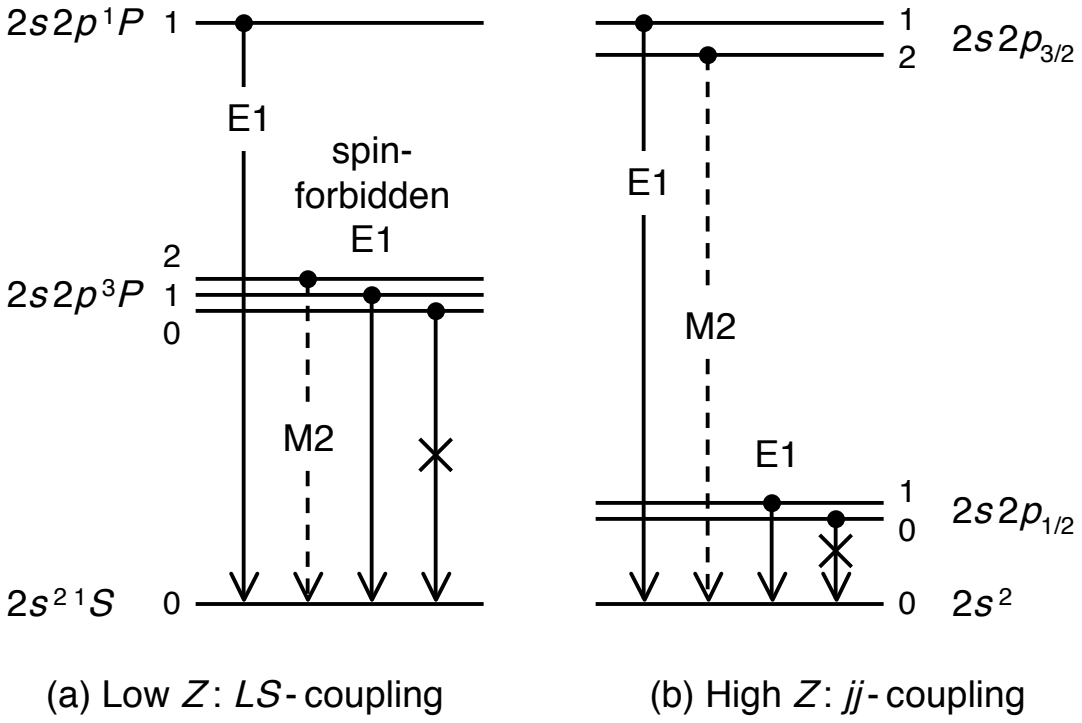

FIG. 1: Low-lying states of Be-like ions at low and high Z.

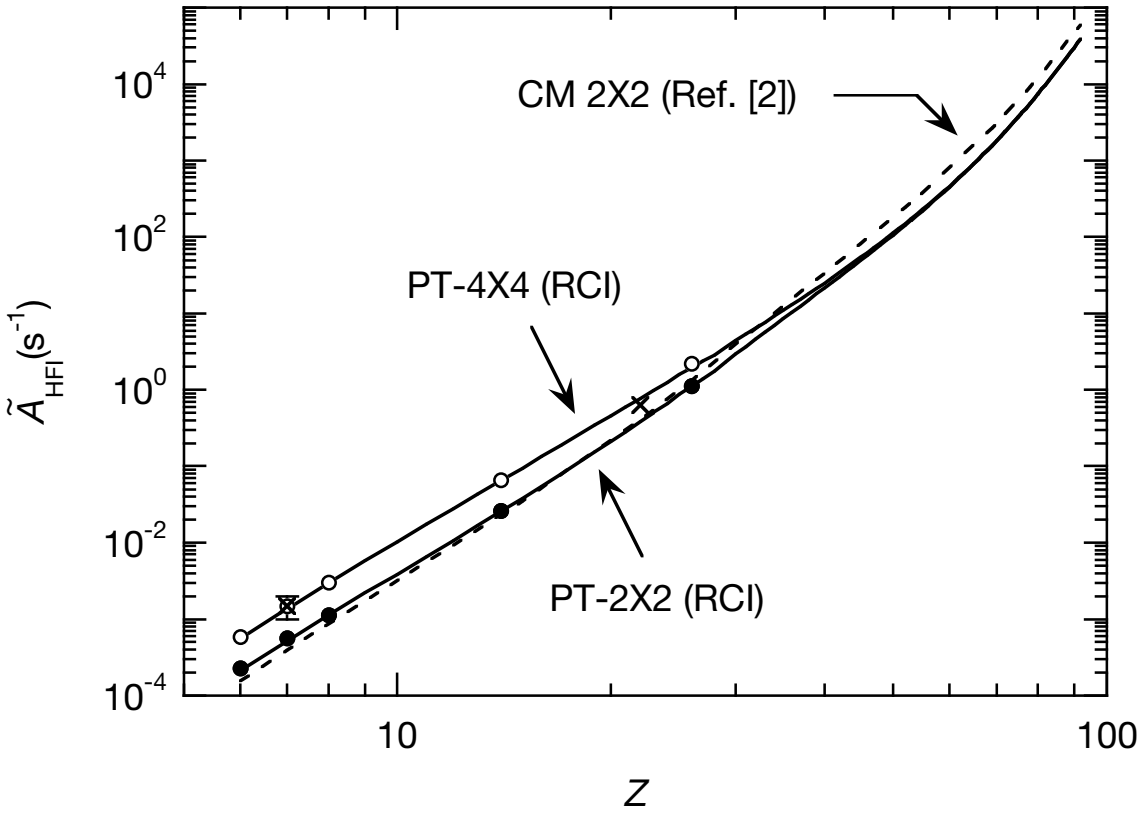

FIG. 2: The scaled hyperfine-induced decay rates for the $2s2p\,^3P_0$ state as functions of the nuclear charge Z. The solid lines are perturbative results of the present work. The dashed line is the complex matrix results of Marques *et al.* [2]. The closed and open circles are the 2×2 and 4×4 perturbative results, respectively, of Brage *et al.* [1] calculated with the correlated MCHF, MCDF and FCI methods. The crosses are experimental data from [3] and [4].

TABLE I: Excitation energies (eV) of the $2s2p\,^{1,3}P$ states from the $2s^2\,^1S_0$ ground state for Be-like ions. Numbers in brackets represent powers of 10.

Z	$E(^3P_0)$	$E(^3P_1)$	$E(^3P_2)$	$E(^1P_1)$	Z	$E(^3P_0)$	$E(^3P_1)$	$E(^3P_2)$	$E(^1P_1)$
6	6.49269[0]	6.49563[0]	6.50261[0]	1.26900[1]	50	9.40357[1]	1.14283[2]	3.55108[2]	4.14007[2]
7	8.33288[0]	8.34070[0]	8.35856[0]	1.62040[1]	51	9.65709[1]	1.17471[2]	3.81106[2]	4.41114[2]
8	1.01596[1]	1.01764[1]	1.02145[1]	1.96884[1]	52	9.91479[1]	1.20692[2]	4.08766[2]	4.69898[2]
9	1.19760[1]	1.20080[1]	1.20790[1]	2.31657[1]	53	1.01794[2]	1.23974[2]	4.38196[2]	5.00468[2]
10	1.37936[1]	1.38500[1]	1.39733[1]	2.66506[1]	54	1.04475[2]	1.27282[2]	4.69449[2]	5.32877[2]
11	1.56070[1]	1.56979[1]	1.58970[1]	3.01539[1]	55	1.07224[2]	1.30650[2]	5.02648[2]	5.67247[2]
12	1.74203[1]	1.75600[1]	1.78650[1]	3.36849[1]	56	1.10021[2]	1.34057[2]	5.37863[2]	6.03650[2]
13	1.92359[1]	1.94405[1]	1.98907[1]	3.72560[1]	57	1.12879[2]	1.37517[2]	5.75207[2]	6.42196[2]
14	2.10528[1]	2.13431[1]	2.19846[1]	4.08750[1]	58	1.15795[2]	1.41027[2]	6.14774[2]	6.82984[2]
15	2.28724[1]	2.32706[1]	2.41591[1]	4.45529[1]	59	1.18774[2]	1.44592[2]	6.56676[2]	7.26121[2]
16	2.46953[1]	2.52276[1]	2.64312[1]	4.83021[1]	60	1.21814[2]	1.48210[2]	7.01018[2]	7.71715[2]
17	2.65218[1]	2.72174[1]	2.88155[1]	5.21355[1]	61	1.24912[2]	1.51878[2]	7.47909[2]	8.19875[2]
18	2.83520[1]	2.92433[1]	3.13287[1]	5.60671[1]	62	1.28066[2]	1.55594[2]	7.97465[2]	8.70717[2]
19	3.01930[1]	3.13080[1]	3.39830[1]	6.01080[1]	63	1.31309[2]	1.59391[2]	8.49841[2]	9.24397[2]
20	3.20240[1]	3.34090[1]	3.68170[1]	6.43010[1]	64	1.34606[2]	1.63234[2]	9.05128[2]	9.81005[2]
21	3.38720[1]	3.55660[1]	3.98290[1]	6.86180[1]	65	1.37991[2]	1.67157[2]	9.63494[2]	1.04071[3]
22	3.57310[1]	3.77681[1]	4.30548[1]	7.31125[1]	66	1.41466[2]	1.71162[2]	1.02508[3]	1.10365[3]
23	3.75796[1]	3.99973[1]	4.64941[1]	7.78001[1]	67	1.44932[2]	1.75150[2]	1.08992[3]	1.16987[3]
24	3.94307[1]	4.22935[1]	5.02161[1]	8.27074[1]	68	1.48608[2]	1.79341[2]	1.15840[3]	1.23974[3]
25	4.13301[1]	4.46306[1]	5.42183[1]	8.78763[1]	69	1.52261[2]	1.83499[2]	1.23042[3]	1.31318[3]
26	4.31688[1]	4.70055[1]	5.84933[1]	9.32869[1]	70	1.56006[2]	1.87742[2]	1.30628[3]	1.39047[3]
27	4.50224[1]	4.94350[1]	6.31340[1]	9.90683[1]	71	1.59863[2]	1.92088[2]	1.38615[3]	1.47180[3]
28	4.68896[1]	5.19147[1]	6.81293[1]	1.05084[2]	72	1.63769[2]	1.96475[2]	1.47016[3]	1.55728[3]
29	4.88374[1]	5.44253[1]	7.35586[1]	1.11510[2]	73	1.67795[2]	2.00972[2]	1.55855[3]	1.64716[3]
30	5.07845[1]	5.69653[1]	7.93816[1]	1.18411[2]	74	1.71845[2]	2.05484[2]	1.65142[3]	1.74155[3]
31	5.27158[1]	5.95543[1]	8.56930[1]	1.25713[2]	75	1.76066[2]	2.10159[2]	1.74913[3]	1.84079[3]
32	5.46617[1]	6.21783[1]	9.25114[1]	1.33505[2]	76	1.80331[2]	2.14867[2]	1.85175[3]	1.94497[3]
33	5.66241[1]	6.48357[1]	9.98759[1]	1.41831[2]	77	1.84682[2]	2.19652[2]	1.95954[3]	2.05434[3]
34	5.86037[1]	6.75237[1]	1.07826[2]	1.50733[2]	78	1.89134[2]	2.24527[2]	2.07275[3]	2.16915[3]
35	6.06034[1]	7.02419[1]	1.16406[2]	1.60259[2]	79	1.93670[2]	2.29476[2]	2.19160[3]	2.28963[3]
36	6.26228[1]	7.29867[1]	1.25656[2]	1.70454[2]	80	1.98247[2]	2.34456[2]	2.31630[3]	2.41597[3]
37	6.46654[1]	7.57590[1]	1.35626[2]	1.81368[2]	81	2.02978[2]	2.39577[2]	2.44722[3]	2.54857[3]
38	6.67326[1]	7.85578[1]	1.46362[2]	1.93052[2]	82	2.07756[2]	2.44734[2]	2.58454[3]	2.68759[3]
39	6.88257[1]	8.13822[1]	1.57913[2]	2.05557[2]	83	2.12599[2]	2.49943[2]	2.72856[3]	2.83332[3]
40	7.09457[1]	8.42316[1]	1.70331[2]	2.18937[2]	84	2.17576[2]	2.55273[2]	2.87966[3]	2.98617[3]
41	7.30945[1]	8.71063[1]	1.83669[2]	2.33246[2]	85	2.22510[2]	2.60547[2]	3.03797[3]	3.14624[3]
42	7.52724[1]	9.00053[1]	1.97982[2]	2.48540[2]	86	2.27429[2]	2.65792[2]	3.20385[3]	3.31391[3]
43	7.74864[1]	9.29347[1]	2.13333[2]	2.64885[2]	87	2.32588[2]	2.71261[2]	3.37793[3]	3.48981[3]
44	7.97321[1]	9.58893[1]	2.29775[2]	2.82335[2]	88	2.37723[2]	2.76692[2]	3.56029[3]	3.67403[3]
45	8.20156[1]	9.88744[1]	2.47377[2]	3.00956[2]	89	2.42978[2]	2.82226[2]	3.75150[3]	3.86711[3]
46	8.43372[1]	1.01890[2]	2.66201[2]	3.20815[2]	90	2.47461[2]	2.86968[2]	3.95097[3]	4.06847[3]
47	8.66990[1]	1.04938[2]	2.86316[2]	3.41979[2]	91	2.53458[2]	2.93209[2]	4.16166[3]	4.28110[3]
48	8.90984[1]	1.08015[2]	3.07787[2]	3.64513[2]	92	2.57564[2]	2.97537[2]	4.38027[3]	4.50166[3]
49	9.15458[1]	1.11132[2]	3.30694[2]	3.88499[2]					

TABLE II: Comparisons between theory and experiment on the excitation energies (eV) of the $2s2p\,^{1,3}P$ states for selected Be-like ions. Experimental energies for $Z = 26 - 42$ are from the NIST Atomic Spectra Database [8]. Those for $Z = 90$ and 92 are from EBIT measurements [26] and [27], respectively.

Z	State	RCI	MP	QED	Theory	Expt	$\Delta E(\%)$
26	$^3P_0$	43.636	-0.011	-0.442	43.183	43.169	0.03
	$^3P_1$	47.453	-0.011	-0.435	47.007	47.006	0.00
	$^3P_2$	58.911	-0.011	-0.406	58.494	58.493	0.00
	$^1P_1$	93.737	-0.011	-0.413	93.314	93.287	0.03
30	$^3P_0$	51.540	-0.013	-0.743	50.785		
	$^3P_1$	57.712	-0.013	-0.734	56.965	56.985	-0.03
	$^3P_2$	80.072	-0.012	-0.678	79.382	79.408	-0.03
	$^1P_1$	119.110	-0.012	-0.687	118.411	118.381	0.02
32	$^3P_0$	55.612	-0.014	-0.937	54.662		
	$^3P_1$	63.119	-0.014	-0.927	62.178	62.191	-0.02
	$^3P_2$	93.377	-0.013	-0.852	92.511	92.527	-0.02
	$^1P_1$	134.381	-0.013	-0.862	133.505	133.457	0.04
36	$^3P_0$	64.067	-0.016	-1.428	62.623	62.674	-0.08
	$^3P_1$	74.420	-0.016	-1.418	72.987	72.998	-0.02
	$^3P_2$	126.963	-0.015	-1.292	125.656	125.651	0.00
	$^1P_1$	171.771	-0.015	-1.302	170.454	170.411	0.02
42	$^3P_0$	77.763	-0.019	-2.471	75.272		
	$^3P_1$	92.486	-0.019	-2.461	90.005	89.983	0.03
	$^3P_2$	200.219	-0.018	-2.220	197.982		
	$^1P_1$	250.788	-0.018	-2.229	248.540	248.445	0.04
90	$^3P_0$	284.98	-0.05	-37.46	247.46		
	$^3P_1$	324.48	-0.05	-37.46	286.97		
	$^3P_2$	3986.01	-0.04	-35.00	3950.97		
	$^1P_1$	4103.51	-0.04	-35.00	4068.47	4068.47(16)	0.00
92	$^3P_0$	298.22	-0.06	-40.60	257.56		
	$^3P_1$	338.20	-0.06	-40.60	297.54		
	$^3P_2$	4418.55	-0.04	-38.24	4380.27		
	$^1P_1$	4539.94	-0.04	-38.24	4501.66	4501.72(27)	0.00

TABLE III: Radiative decay rates (s^{-1}) to the $2s^2\ ^1S_0$ ground state for Be-like ions. Numbers in brackets represent powers of 10.

Z	$A_{\rm E1}(^3P_1)$	$A_{\rm M2}(^3P_2)$	$A_{\rm E1}(^1P_1)$	Z	$A_{\rm E1}(^3P_1)$	$A_{\rm M2}(^3P_2)$	$A_{\rm E1}(^1P_1)$
6	1.003[2]	5.151[-3]	1.763[9]	50	1.676[9]	1.373[4]	3.825[11]
7	5.662[2]	1.145[-2]	2.317[9]	51	1.791[9]	1.865[4]	4.420[11]
8	2.241[3]	2.152[-2]	2.865[9]	52	1.909[9]	2.529[4]	5.110[11]
9	7.050[3]	3.636[-2]	3.419[9]	53	2.030[9]	3.422[4]	5.909[11]
10	1.887[4]	5.742[-2]	3.983[9]	54	2.154[9]	4.620[4]	6.833[11]
11	4.466[4]	8.613[-2]	4.559[9]	55	2.281[9]	6.225[4]	7.902[11]
12	9.623[4]	1.246[-1]	5.150[9]	56	2.411[9]	8.368[4]	9.137[11]
13	1.923[5]	1.756[-1]	5.764[9]	57	2.545[9]	1.122[5]	1.056[12]
14	3.615[5]	2.425[-1]	6.405[9]	58	2.682[9]	1.502[5]	1.221[12]
15	6.454[5]	3.300[-1]	7.078[9]	59	2.823[9]	2.005[5]	1.411[12]
16	1.103[6]	4.444[-1]	7.791[9]	60	2.967[9]	2.671[5]	1.630[12]
17	1.817[6]	5.940[-1]	8.551[9]	61	3.115[9]	3.550[5]	1.881[12]
18	2.895[6]	7.901[-1]	9.365[9]	62	3.266[9]	4.707[5]	2.171[12]
19	4.480[6]	1.047[0]	1.024[10]	63	3.422[9]	6.227[5]	2.504[12]
20	6.751[6]	1.388[0]	1.120[10]	64	3.582[9]	8.218[5]	2.886[12]
21	9.943[6]	1.838[0]	1.224[10]	65	3.747[9]	1.082[6]	3.325[12]
22	1.432[7]	2.438[0]	1.338[10]	66	3.918[9]	1.422[6]	3.828[12]
23	2.019[7]	3.232[0]	1.464[10]	67	4.087[9]	1.864[6]	4.404[12]
24	2.795[7]	4.307[0]	1.604[10]	68	4.272[9]	2.439[6]	5.064[12]
25	3.799[7]	5.753[0]	1.761[10]	69	4.453[9]	3.184[6]	5.818[12]
26	5.073[7]	7.682[0]	1.935[10]	70	4.641[9]	4.147[6]	6.680[12]
27	6.667[7]	1.031[1]	2.134[10]	71	4.836[9]	5.390[6]	7.665[12]
28	8.629[7]	1.388[1]	2.352[10]	72	5.034[9]	6.992[6]	8.787[12]
29	1.099[8]	1.878[1]	2.602[10]	73	5.240[9]	9.052[6]	1.007[13]
30	1.380[8]	2.541[1]	2.890[10]	74	5.447[9]	1.169[7]	1.152[13]
31	1.709[8]	3.452[1]	3.215[10]	75	5.666[9]	1.508[7]	1.318[13]
32	2.088[8]	4.701[1]	3.587[10]	76	5.888[9]	1.941[7]	1.507[13]
33	2.519[8]	6.418[1]	4.012[10]	77	6.114[9]	2.493[7]	1.722[13]
34	3.003[8]	8.780[1]	4.501[10]	78	6.348[9]	3.197[7]	1.965[13]
35	3.539[8]	1.203[2]	5.063[10]	79	6.586[9]	4.093[7]	2.242[13]
36	4.128[8]	1.651[2]	5.712[10]	80	6.826[9]	5.229[7]	2.555[13]
37	4.767[8]	2.268[2]	6.460[10]	81	7.077[9]	6.671[7]	2.911[13]
38	5.456[8]	3.118[2]	7.326[10]	82	7.329[9]	8.496[7]	3.313[13]
39	6.191[8]	4.289[2]	8.328[10]	83	7.584[9]	1.080[8]	3.768[13]
40	6.971[8]	5.901[2]	9.489[10]	84	7.848[9]	1.372[8]	4.284[13]
41	7.793[8]	8.117[2]	1.083[11]	85	8.103[9]	1.738[8]	4.866[13]
42	8.654[8]	1.116[3]	1.240[11]	86	8.352[9]	2.200[8]	5.523[13]
43	9.553[8]	1.534[3]	1.421[11]	87	8.619[9]	2.781[8]	6.266[13]
44	1.049[9]	2.106[3]	1.631[11]	88	8.879[9]	3.510[8]	7.104[13]
45	1.145[9]	2.889[3]	1.875[11]	89	9.144[9]	4.424[8]	8.050[13]
46	1.246[9]	3.957[3]	2.158[11]	90	9.322[9]	5.564[8]	9.109[13]
47	1.349[9]	5.414[3]	2.487[11]	91	9.651[9]	7.002[8]	1.032[14]
48	1.455[9]	7.395[3]	2.869[11]	92	9.773[9]	8.780[8]	1.166[14]
49	1.564[9]	1.008[4]	3.312[11]				

TABLE IV: Comparisons between theory and experiment on the radiative decay rates (s^{-1}) of the $2s2p\ ^{1,3}P_1 - 2s^2\ ^1S_0$ transitions for selected Be-like ions. RCI are results of this work. Numbers in brackets represent powers of 10.

Transition	Work	$Z = 6$	7	8	14	22	26	42
$^3P_1 - {}^1S_0$	RCI	1.02[2]	5.66[2]	2.24[3]	3.61[5]	1.43[7]	5.07[7]	8.65[8]
	MCDF[a]	1.00[2]	5.64[2]	2.21[3]	3.59[5]		5.19[7]	9.37[8]
	CIV3[b]	1.04[2]	4.95[2]	1.99[3]	3.48[5]			
	MCDF[c]	7.95[1]	4.71[2]	1.93[3]	3.37[5]	1.38[7]	4.95[7]	8.65[8]
	Expt	1.03[2][d]						
$^1P_1 - {}^1S_0$	RCI	1.76[9]	2.32[9]	2.86[9]	6.41[9]	1.34[10]	1.93[10]	1.24[11]
	MCDF[a]	1.78[9]	2.33[9]	2.87[9]	6.45[9]		1.96[10]	1.27[11]
	CIV3[b]	1.76[9]	2.35[9]	2.90[9]				
	Expt	1.76[9][e]	2.35[9][f]	2.97[9][f]	6.67[9][g]		1.89[10][h]	

[a]Ynnerman and Froese Fischer [24].
[b]Fleming *et al.* [28].
[c]Marques *et al.* [2].
[d]Doerfert *et al.* [23].
[e]Reistad and Martinson [29] and Träbert [30].
[f]Engström *et al.* [31].
[g]Träbert and Heckmann [32].
[h]Buchet *et al.* [33].

TABLE V: Reduced M1 hyperfine matrix elements $T(a,b) = \langle a \| T^{(1)} \| b \rangle$ (a.u.) between the ^3P_J states of Be-like ions. Numbers in brackets represent powers of 10.

Z	$T(^3P_0, ^3P_1)$	$T(^3P_1, ^3P_1)$	$T(^3P_1, ^3P_2)$	$T(^3P_2, ^3P_2)$	Z	$T(^3P_0, ^3P_1)$	$T(^3P_1, ^3P_1)$	$T(^3P_1, ^3P_2)$	$T(^3P_2, ^3P_2)$
6	-1.3689[-1]	2.0890[-1]	1.8398[-1]	3.9512[-1]	50	-2.1859[2]	5.9266[2]	3.6801[1]	5.9132[2]
7	-2.3954[-1]	3.8515[-1]	3.2654[-1]	7.1946[-1]	51	-2.3542[2]	6.3919[2]	3.6247[1]	6.3533[2]
8	-3.8305[-1]	6.3994[-1]	5.2750[-1]	1.1832[0]	52	-2.5324[2]	6.8849[2]	3.5601[1]	6.8189[2]
9	-5.7450[-1]	9.8885[-1]	7.9629[-1]	1.8110[0]	53	-2.7225[2]	7.4097[2]	3.4894[1]	7.3143[2]
10	-8.2134[-1]	1.4487[0]	1.1420[0]	2.6283[0]	54	-2.9233[2]	7.9649[2]	3.4089[1]	7.8373[2]
11	-1.1313[0]	2.0378[0]	1.5730[0]	3.6604[0]	55	-3.1368[2]	8.5546[2]	3.3213[1]	8.3922[2]
12	-1.5128[0]	2.7763[0]	2.0972[0]	4.9336[0]	56	-3.3624[2]	9.1789[2]	3.2246[1]	8.9785[2]
13	-1.9746[0]	3.6867[0]	2.7210[0]	6.4743[0]	57	-3.6024[2]	9.8420[2]	3.1211[1]	9.6004[2]
14	-2.5263[0]	4.7942[0]	3.4503[0]	8.3098[0]	58	-3.8568[2]	1.0545[3]	3.0097[1]	1.0259[3]
15	-3.1779[0]	6.1270[0]	4.2890[0]	1.0467[1]	59	-4.1267[2]	1.1291[3]	2.8907[1]	1.0956[3]
16	-3.9408[0]	7.7169[0]	5.2399[0]	1.2976[1]	60	-4.4117[2]	1.2080[3]	2.7625[1]	1.1692[3]
17	-4.8262[0]	9.5991[0]	6.3034[0]	1.5864[1]	61	-4.7148[2]	1.2918[3]	2.6276[1]	1.2473[3]
18	-5.8470[0]	1.1813[1]	7.4782[0]	1.9161[1]	62	-5.0338[2]	1.3803[3]	2.4823[1]	1.3295[3]
19	-7.0180[0]	1.4404[1]	8.7617[0]	2.2901[1]	63	-5.3736[2]	1.4745[3]	2.3309[1]	1.4168[3]
20	-8.3526[0]	1.7418[1]	1.0147[1]	2.7111[1]	64	-5.7314[2]	1.5739[3]	2.1691[1]	1.5088[3]
21	-9.8652[0]	2.0906[1]	1.1624[1]	3.1824[1]	65	-6.1125[2]	1.6797[3]	2.0011[1]	1.6065[3]
22	-1.1574[1]	2.4926[1]	1.3183[1]	3.7075[1]	66	-6.5150[2]	1.7916[3]	1.8235[1]	1.7097[3]
23	-1.3494[1]	2.9534[1]	1.4811[1]	4.2898[1]	67	-6.9421[2]	1.9104[3]	1.6382[1]	1.8190[3]
24	-1.5646[1]	3.4794[1]	1.6492[1]	4.9330[1]	68	-7.3947[2]	2.0364[3]	1.4443[1]	1.9347[3]
25	-1.8044[1]	4.0764[1]	1.8208[1]	5.6406[1]	69	-7.8747[2]	2.1702[3]	1.2421[1]	2.0573[3]
26	-2.0709[1]	4.7510[1]	1.9942[1]	6.4167[1]	70	-8.3810[2]	2.3118[3]	1.0292[1]	2.1866[3]
27	-2.3658[1]	5.5091[1]	2.1671[1]	7.2649[1]	71	-8.9196[2]	2.4624[3]	8.0879[0]	2.3239[3]
28	-2.6913[1]	6.3571[1]	2.3382[1]	8.1901[1]	72	-9.4885[2]	2.6219[3]	5.7790[0]	2.4690[3]
29	-3.0485[1]	7.3001[1]	2.5048[1]	9.1951[1]	73	-1.0093[3]	2.7915[3]	3.3845[0]	2.6229[3]
30	-3.4401[1]	8.3444[1]	2.6658[1]	1.0286[2]	74	-1.0732[3]	2.9715[3]	8.9002[-1]	2.7858[3]
31	-3.8672[1]	9.4948[1]	2.8192[1]	1.1466[2]	75	-1.1411[3]	3.1628[3]	-1.6972[0]	2.9585[3]
32	-4.3323[1]	1.0757[2]	2.9641[1]	1.2741[2]	76	-1.2127[3]	3.3658[3]	-4.4009[0]	3.1411[3]
33	-4.8372[1]	1.2136[2]	3.0991[1]	1.4117[2]	77	-1.2890[3]	3.5820[3]	-7.1864[0]	3.3352[3]
34	-5.3835[1]	1.3635[2]	3.2233[1]	1.5597[2]	78	-1.3697[3]	3.8117[3]	-1.0085[1]	3.5407[3]
35	-5.9742[1]	1.5262[2]	3.3365[1]	1.7189[2]	79	-1.4555[3]	4.0565[3]	-1.3078[1]	3.7591[3]
36	-6.6100[1]	1.7019[2]	3.4376[1]	1.8896[2]	80	-1.5460[3]	4.3162[3]	-1.6201[1]	3.9900[3]
37	-7.2945[1]	1.8914[2]	3.5269[1]	2.0727[2]	81	-1.6419[3]	4.5926[3]	-1.9439[1]	4.2348[3]
38	-8.0293[1]	2.0951[2]	3.6042[1]	2.2688[2]	82	-1.7438[3]	4.8874[3]	-2.2778[1]	4.4951[3]
39	-8.8175[1]	2.3138[2]	3.6696[1]	2.4785[2]	83	-1.8523[3]	5.2018[3]	-2.6219[1]	4.7719[3]
40	-9.6608[1]	2.5478[2]	3.7231[1]	2.7024[2]	84	-1.9679[3]	5.5380[3]	-2.9748[1]	5.0671[3]
41	-1.0563[2]	2.7981[2]	3.7652[1]	2.9415[2]	85	-2.0903[3]	5.8959[3]	-3.3410[1]	5.3801[3]
42	-1.1526[2]	3.0653[2]	3.7959[1]	3.1963[2]	86	-2.2153[3]	6.2693[3]	-3.7386[1]	5.7044[3]
43	-1.2553[2]	3.3504[2]	3.8159[1]	3.4679[2]	87	-2.3526[3]	6.6755[3]	-4.1299[1]	6.0572[3]
44	-1.3648[2]	3.6540[2]	3.8253[1]	3.7568[2]	88	-2.4972[3]	7.1068[3]	-4.5375[1]	6.4305[3]
45	-1.4816[2]	3.9774[2]	3.8248[1]	4.0644[2]	89	-2.6517[3]	7.5687[3]	-4.9537[1]	6.8293[3]
46	-1.6057[2]	4.3212[2]	3.8142[1]	4.3911[2]	90	-2.8130[3]	8.0570[3]	-5.3914[1]	7.2491[3]
47	-1.7380[2]	4.6872[2]	3.7946[1]	4.7386[2]	91	-2.9879[3]	8.5845[3]	-5.8286[1]	7.7027[3]
48	-1.8782[2]	5.0755[2]	3.7650[1]	5.1070[2]	92	-3.1676[3]	9.1366[3]	-6.2981[1]	8.1749[3]
49	-2.0275[2]	5.4884[2]	3.7271[1]	5.4984[2]					

TABLE VI: Reduced M1 hyperfine matrix elements $T(a,b) = \langle a \| T^{(1)} \| b \rangle$ (a.u.) between the $^1P_1$ and $^{1,3}P_J$ states of Be-like ions. Numbers in brackets represent powers of 10.

Z	$T(^1P_1, ^3P_0)$	$T(^1P_1, ^3P_1)$	$T(^1P_1, ^3P_2)$	$T(^1P_1, ^1P_1)$	Z	$T(^1P_1, ^3P_0)$	$T(^1P_1, ^3P_1)$	$T(^1P_1, ^3P_2)$	$T(^1P_1, ^1P_1)$
6	1.1553[-1]	-2.5496[-1]	3.0203[-1]	4.9220[-2]	50	4.4050[1]	-1.0981[2]	4.9026[2]	-1.5887[2]
7	2.0118[-1]	-4.5910[-1]	5.3676[-1]	9.8814[-2]	51	4.5606[1]	-1.1252[2]	5.2786[2]	-1.7307[2]
8	3.2110[-1]	-7.4816[-1]	8.6976[-1]	1.7070[-1]	52	4.7202[1]	-1.1524[2]	5.6772[2]	-1.8815[2]
9	4.8049[-1]	-1.1364[0]	1.3180[0]	2.6783[-1]	53	4.8860[1]	-1.1802[2]	6.1023[2]	-2.0426[2]
10	6.8446[-1]	-1.6383[0]	1.8992[0]	3.9219[-1]	54	5.0560[1]	-1.2081[2]	6.5522[2]	-2.2134[2]
11	9.3786[-1]	-2.2680[0]	2.6318[0]	5.4453[-1]	55	5.2320[1]	-1.2366[2]	7.0306[2]	-2.3954[2]
12	1.2454[0]	-3.0393[0]	3.5353[0]	7.2397[-1]	56	5.4132[1]	-1.2654[2]	7.5373[2]	-2.5885[2]
13	1.6112[0]	-3.9655[0]	4.6299[0]	9.2771[-1]	57	5.6012[1]	-1.2950[2]	8.0761[2]	-2.7944[2]
14	2.0391[0]	-5.0594[0]	5.9376[0]	1.1506[0]	58	5.7956[1]	-1.3253[2]	8.6481[2]	-3.0136[2]
15	2.5324[0]	-6.3324[0]	7.4810[0]	1.3850[0]	59	5.9969[1]	-1.3563[2]	9.2552[2]	-3.2468[2]
16	3.0936[0]	-7.7952[0]	9.2852[0]	1.6199[0]	60	6.2045[1]	-1.3879[2]	9.8978[2]	-3.4943[2]
17	3.7245[0]	-9.4560[0]	1.1376[1]	1.8414[0]	61	6.4202[1]	-1.4206[2]	1.0581[3]	-3.7582[2]
18	4.4257[0]	-1.1322[1]	1.3780[1]	2.0318[0]	62	6.6420[1]	-1.4538[2]	1.1303[3]	-4.0375[2]
19	5.1982[0]	-1.3398[1]	1.6530[1]	2.1698[0]	63	6.8728[1]	-1.4882[2]	1.2071[3]	-4.3359[2]
20	6.0401[0]	-1.5684[1]	1.9655[1]	2.2309[0]	64	7.1106[1]	-1.5234[2]	1.2883[3]	-4.6518[2]
21	6.9488[0]	-1.8177[1]	2.3186[1]	2.1874[0]	65	7.3581[1]	-1.5599[2]	1.3747[3]	-4.9894[2]
22	7.9218[0]	-2.0874[1]	2.7160[1]	2.0083[0]	66	7.6137[1]	-1.5974[2]	1.4662[3]	-5.3477[2]
23	8.9547[0]	-2.3763[1]	3.1611[1]	1.6606[0]	67	7.8788[1]	-1.6363[2]	1.5634[3]	-5.7295[2]
24	1.0043[1]	-2.6832[1]	3.6579[1]	1.1099[0]	68	8.1535[1]	-1.6764[2]	1.6666[3]	-6.1359[2]
25	1.1179[1]	-3.0061[1]	4.2097[1]	3.2202[-1]	69	8.4383[1]	-1.7179[2]	1.7762[3]	-6.5688[2]
26	1.2358[1]	-3.3431[1]	4.8207[1]	-7.3782[-1]	70	8.7322[1]	-1.7606[2]	1.8921[3]	-7.0280[2]
27	1.3571[1]	-3.6914[1]	5.4944[1]	-2.1010[0]	71	9.0377[1]	-1.8050[2]	2.0155[3]	-7.5185[2]
28	1.4814[1]	-4.0488[1]	6.2353[1]	-3.7991[0]	72	9.3533[1]	-1.8507[2]	2.1463[3]	-8.0396[2]
29	1.6076[1]	-4.4117[1]	7.0460[1]	-5.8553[0]	73	9.6808[1]	-1.8983[2]	2.2853[3]	-8.5955[2]
30	1.7354[1]	-4.7783[1]	7.9320[1]	-8.2958[0]	74	1.0020[2]	-1.9475[2]	2.4329[3]	-9.1873[2]
31	1.8640[1]	-5.1451[1]	8.8959[1]	-1.1137[1]	75	1.0371[2]	-1.9986[2]	2.5898[3]	-9.8186[2]
32	1.9932[1]	-5.5103[1]	9.9429[1]	-1.4396[1]	76	1.0734[2]	-2.0514[2]	2.7561[3]	-1.0489[3]
33	2.1225[1]	-5.8717[1]	1.1077[2]	-1.8086[1]	77	1.1112[2]	-2.1064[2]	2.9334[3]	-1.1207[3]
34	2.2516[1]	-6.2271[1]	1.2302[2]	-2.2214[1]	78	1.1502[2]	-2.1634[2]	3.1216[3]	-1.1972[3]
35	2.3806[1]	-6.5760[1]	1.3623[2]	-2.6794[1]	79	1.1907[2]	-2.2227[2]	3.3221[3]	-1.2789[3]
36	2.5091[1]	-6.9165[1]	1.5044[2]	-3.1827[1]	80	1.2325[2]	-2.2840[2]	3.5346[3]	-1.3658[3]
37	2.6375[1]	-7.2488[1]	1.6572[2]	-3.7330[1]	81	1.2757[2]	-2.3476[2]	3.7605[3]	-1.4585[3]
38	2.7658[1]	-7.5724[1]	1.8210[2]	-4.3307[1]	82	1.3206[2]	-2.4139[2]	4.0013[3]	-1.5576[3]
39	2.8943[1]	-7.8875[1]	1.9966[2]	-4.9772[1]	83	1.3671[2]	-2.4829[2]	4.2581[3]	-1.6637[3]
40	3.0230[1]	-8.1942[1]	2.1844[2]	-5.6734[1]	84	1.4154[2]	-2.5550[2]	4.5326[3]	-1.7774[3]
41	3.1525[1]	-8.4934[1]	2.3852[2]	-6.4214[1]	85	1.4653[2]	-2.6297[2]	4.8244[3]	-1.8987[3]
42	3.2828[1]	-8.7854[1]	2.5995[2]	-7.2224[1]	86	1.5157[2]	-2.7045[2]	5.1269[3]	-2.0246[3]
43	3.4146[1]	-9.0715[1]	2.8282[2]	-8.0795[1]	87	1.5689[2]	-2.7849[2]	5.4572[3]	-2.1626[3]
44	3.5480[1]	-9.3521[1]	3.0720[2]	-8.9942[1]	88	1.6236[2]	-2.8678[2]	5.8074[3]	-2.3091[3]
45	3.6836[1]	-9.6290[1]	3.3319[2]	-9.9706[1]	89	1.6803[2]	-2.9544[2]	6.1825[3]	-2.4663[3]
46	3.8215[1]	-9.9020[1]	3.6084[2]	-1.1010[2]	90	1.7382[2]	-3.0428[2]	6.5778[3]	-2.6321[3]
47	3.9625[1]	-1.0173[2]	3.9030[2]	-1.2119[2]	91	1.7986[2]	-3.1364[2]	7.0061[3]	-2.8118[3]
48	4.1062[1]	-1.0442[2]	4.2158[2]	-1.3297[2]	92	1.8597[2]	-3.2305[2]	7.4521[3]	-2.9987[3]
49	4.2538[1]	-1.0712[2]	4.5489[2]	-1.4552[2]					

TABLE VII: Hyperfine-induced $2s2p\,^3P_0 - 2s^2\,^1S_0$ transition rates (s^{-1}) for Be-like ions. Nuclear magnetic moments μ_I are from [25]. Numbers in brackets represent powers of 10.

Z	Isotope	I	μ_I	$A_{\rm HFI}$	Z	Isotope	I	μ_I	$A_{\rm HFI}$	Z	Isotope	I	μ_I	$A_{\rm HFI}$
6	^{13}C	1/2	0.70241	8.223[-4]	38	^{87}Sr	9/2	-1.0936	2.643[1]	63	^{154}Eu	3	-2.005	3.719[3]
7	^{14}N	1	0.40376	4.440[-4]	39	^{89}Y	1/2	-0.13742	1.205[0]	64	^{155}Gd	3/2	-0.2581	8.848[1]
7	^{15}N	1/2	-0.28319	3.269[-4]	40	^{91}Zr	5/2	-1.3036	5.934[1]	64	^{157}Gd	3/2	-0.3386	1.523[2]
8	^{17}O	5/2	-1.8938	1.488[-2]	41	^{93}Nb	9/2	6.1705	1.361[3]	65	^{157}Tb	3/2	2.0	6.126[3]
9	^{19}F	1/2	2.6289	1.208[-1]	42	^{95}Mo	5/2	-0.9142	3.992[1]	65	^{158}Tb	3	1.758	3.780[3]
10	^{21}Ne	3/2	-0.6618	7.453[-3]	42	^{97}Mo	5/2	-0.9335	4.162[1]	65	^{159}Tb	3/2	2.014	6.212[3]
11	^{23}Na	3/2	2.2176	1.431[-1]	43	^{99}Tc	9/2	5.6847	1.574[3]	66	^{161}Dy	5/2	-0.4804	3.397[2]
12	^{25}Mg	5/2	-0.85545	2.871[-2]	44	^{99}Ru	5/2	-0.6413	2.667[1]	66	^{163}Dy	5/2	0.6726	6.667[2]
13	^{27}Al	5/2	3.6415	8.094[-1]	44	^{101}Ru	5/2	-0.7188	3.350[1]	67	^{163}Ho	7/2	4.23	2.784[4]
14	^{29}Si	1/2	-0.55529	6.011[-2]	45	^{103}Rh	1/2	-0.0884	1.262[0]	67	^{165}Ho	7/2	4.173	2.710[4]
15	^{31}P	1/2	1.1316	3.648[-1]	46	^{105}Pd	5/2	-0.642	3.606[1]	68	^{167}Er	7/2	-0.56385	5.669[2]
16	^{33}S	3/2	0.64382	9.315[-2]	47	^{107}Ag	1/2	-0.11368	2.809[0]	69	^{168}Tm	3	0.277	1.630[2]
17	^{35}Cl	3/2	0.82187	2.113[-1]	47	^{109}Ag	1/2	-0.13069	3.712[0]	69	^{169}Tm	1/2	-0.2316	2.559[2]
17	^{36}Cl	2	1.28547	4.652[-1]	48	^{111}Cd	1/2	-0.59489	8.893[1]	70	^{171}Yb	1/2	0.4937	1.341[3]
17	^{37}Cl	3/2	0.68412	1.464[-1]	48	^{113}Cd	1/2	-0.6223	9.730[1]	70	^{173}Yb	5/2	-0.6799	1.182[3]
19	^{39}K	3/2	0.39149	8.873[-2]	49	^{113}In	9/2	5.5289	3.630[3]	71	^{175}Lu	7/2	2.238	1.356[4]
19	^{40}K	4	-1.2981	7.314[-1]	49	^{115}In	9/2	5.5408	3.646[3]	71	^{176}Lu	7	3.1692	2.415[4]
19	^{41}K	3/2	0.21488	2.673[-2]	50	^{115}Sn	1/2	-0.91883	2.832[2]	72	^{177}Hf	7/2	0.7935	1.954[3]
20	^{41}Ca	7/2	-1.5948	1.496[0]	50	^{117}Sn	1/2	-1.001	3.361[2]	72	^{179}Hf	9/2	-0.6409	1.210[3]
20	^{43}Ca	7/2	-1.3176	1.021[0]	50	^{119}Sn	1/2	-1.0473	3.678[2]	73	^{181}Ta	7/2	2.3705	2.008[4]
21	^{45}Sc	7/2	4.7565	1.737[1]	51	^{121}Sb	5/2	-3.3634	2.045[3]	74	^{183}W	1/2	0.11778	1.326[2]
22	^{47}Ti	5/2	-0.78848	6.727[-1]	51	^{123}Sb	7/2	2.5498	1.083[3]	75	^{185}Re	5/2	3.1871	5.236[4]
22	^{49}Ti	7/2	-1.1042	1.212[0]	52	^{123}Te	1/2	-0.73695	2.425[2]	75	^{187}Re	5/2	3.2197	5.344[4]
23	^{50}V	6	3.3457	1.294[1]	52	^{125}Te	1/2	-0.8885	3.523[2]	76	^{187}Os	1/2	0.064652	5.281[1]
23	^{51}V	7/2	5.1487	3.379[1]	53	^{127}I	5/2	2.8133	1.909[3]	76	^{189}Os	3/2	0.65993	3.061[3]
24	^{53}Cr	3/2	-0.47454	4.657[-1]	53	^{129}I	7/2	2.621	1.521[3]	77	^{191}Ir	3/2	0.1484	1.778[2]
25	^{51}Mn	5/2	3.5683	2.825[1]	54	^{129}Xe	1/2	-0.77798	3.588[2]	77	^{193}Ir	3/2	0.1614	2.103[2]
25	^{55}Mn	5/2	3.4687	2.670[1]	54	^{131}Xe	3/2	0.69186	1.581[2]	78	^{195}Pt	1/2	0.60952	6.243[3]
26	^{57}Fe	1/2	0.09062	4.783[-2]	55	^{133}Cs	7/2	2.5826	1.958[3]	79	^{197}Au	3/2	0.14816	2.346[2]
27	^{59}Co	7/2	4.627	6.522[1]	55	^{135}Cs	7/2	2.7324	2.192[3]	80	^{199}Hg	1/2	0.50588	5.687[3]
28	^{61}Ni	3/2	-0.75002	2.698[0]	56	^{133}Ba	1/2	0.77167	4.700[2]	80	^{201}Hg	3/2	-0.56022	3.846[3]
29	^{63}Cu	3/2	2.2273	2.963[1]	56	^{135}Ba	3/2	0.83863	3.079[2]	81	^{203}Tl	1/2	1.6222	6.816[4]
29	^{65}Cu	3/2	2.3816	3.388[1]	56	^{137}Ba	3/2	0.93735	3.847[2]	81	^{205}Tl	1/2	1.6382	6.953[4]
30	^{67}Zn	5/2	0.8752	4.732[0]	57	^{138}La	5	3.7136	5.002[3]	82	^{205}Pb	5/2	0.7117	6.932[3]
31	^{69}Ga	3/2	2.0166	3.620[1]	57	^{139}La	7/2	2.783	3.010[3]	82	^{207}Pb	1/2	0.59258	1.035[4]
31	^{71}Ga	3/2	2.5623	5.845[1]	59	^{141}Pr	5/2	4.2754	1.025[4]	83	^{209}Bi	9/2	4.1106	2.333[5]
32	^{73}Ge	9/2	-0.87947	6.072[0]	60	^{143}Nd	7/2	-1.065	6.685[2]	88	^{223}Ra	3/2	0.2705	2.760[3]
33	^{75}As	3/2	1.4395	2.661[1]	60	^{145}Nd	7/2	-0.656	2.537[2]	89	^{227}Ac	3/2	1.1	5.281[4]
34	^{77}Se	1/2	0.53504	7.902[0]	61	^{147}Pm	7/2	2.58	4.517[3]	90	^{229}Th	5/2	0.46	8.785[3]
35	^{79}Br	3/2	2.1064	8.099[1]	62	^{147}Sm	7/2	-0.8148	5.160[2]	91	^{231}Pa	3/2	2.01	2.346[5]
35	^{81}Br	3/2	2.2706	9.411[1]	62	^{149}Sm	7/2	-0.6715	3.505[2]	92	^{233}U	5/2	0.59	1.899[4]
36	^{83}Kr	9/2	-0.97067	1.494[1]	62	^{151}Sm	5/2	-0.363	1.115[2]	92	^{235}U	7/2	-0.39	7.594[3]
37	^{85}Rb	5/2	1.3534	3.935[1]	63	^{151}Eu	5/2	3.4717	1.176[4]					
37	^{87}Rb	3/2	2.7515	1.938[2]	63	^{153}Eu	5/2	1.533	2.289[3]					

TABLE VIII: The scaled hyperfine-induced transition rates $\tilde{A}_{\rm HFI}(^3P_0) = A_{\rm HFI}(^3P_0)/\mu^2(1+1/I)$ (s^{-1}) are compared between theory and experiment. PT and CM refer to perturbative and complex matrix results, respectively, and 2×2 and 4×4 are hyperfine matrices used in the calculations. RCI are results of this work. Numbers in parentheses are experimental uncertainties. Numbers in brackets represent powers of 10.

Method	Work	$Z=6$	7	8	14	22	26	48	70	92
PT-2×2	RCI	2.13[-4]	5.17[-4]	1.13[-3]	2.56[-2]	0.382	1.12	7.83[1]	1.82[3]	3.88[4]
	MCHF[a]	2.28[-4]	5.72[-4]	1.14[-3]						
	MCDF[a]	2.65[-4]		1.12[-3]	2.61[-2]		1.13			
PT-4×4	RCI	5.56[-4]	1.36[-3]	2.96[-3]	6.50[-2]	0.773	1.94	8.38[1]	1.83[3]	3.88[4]
	MCHF[a]	5.86[-4]	1.49[-3]	3.03[-3]						
	MCDF[a]	6.35[-4]		2.94[-3]	6.56[-2]		2.22			
	FCI[a]	6.11[-4]	1.50[-3]							
CM-2×2	RCI	2.13[-4]	5.18[-4]	1.13[-3]	2.67[-2]	0.451	1.44	1.40[2]	3.16[3]	6.00[4]
	MCDF[b]	1.55[-4]	3.94[-4]	8.74[-4]	2.33[-2]	0.409	1.33	1.33[2]	3.07[3]	5.97[4]
CM-4×4	RCI	8.14[-4]	2.00[-3]	4.30[-3]	9.26[-2]	1.036	2.59	1.46[2]	3.20[3]	6.02[4]
	Expt		1.5(5)[-3][c]			0.64(3)[d]				

[a]Brage *et al.* [1].
[b]Marques *et al.* [2].
[c]Brage *et al.* [3].
[d]Schippers *et al.* [4].